Nanoscale

Accepted Manuscript

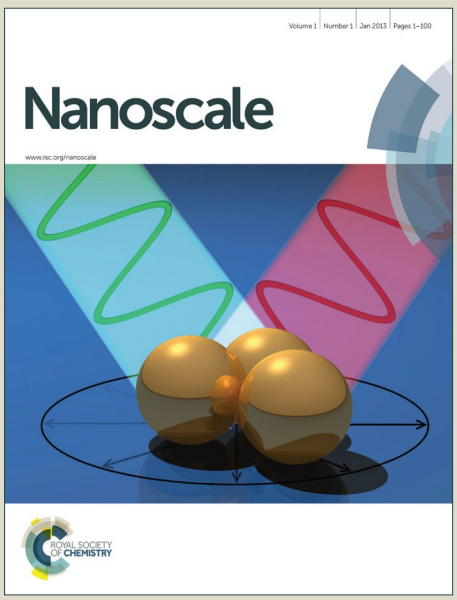

ROYAL SOCIETY OF CHEMISTRY

www.rsc.org/nanoscale

On the mineral core of ferritin-like proteins: a structural and magnetic characterization

A. García-Prieto[1,2], J. Alonso[2,3], D. Muñoz[4,5],
L. Marcano[5], A. Abad Díaz de Cerio[4,5], R. Fernández de Luis[2],
I. Orue[6], O. Mathon[7], A. Muela[2,4], M.L. Fdez-Gubieda[2,5]

[1] Dpto. de Física Aplicada I, Universidad del País Vasco - UPV/EHU, 48013 Bilbao, Spain
[2] BCMaterials, Parque tecnológico de Zamudio, 48160 Derio, Spain
[3] Department of Physics, University of South Florida, Tampa, FL 33647, USA
[4] Dpto. de Inmunología, Microbiología y Parasitología,
Universidad del País Vasco - UPV/EHU, 48940 Leioa, Spain
[5] Dpto. de Electricidad y Electrónica, Universidad del País Vasco - UPV/EHU, 48940 Leioa, Spain
[6] SGIker, Universidad del País Vasco UPV/EHU, 48940 Leioa, Spain
[7] European Synchrotron Radiation Facility, 38000 Grenoble, France

October 9, 2015

It is generally accepted that the mineral core synthesized by ferritin-like proteins consists of a ferric oxy-hydroxide mineral similar to ferrihydrite in the case of horse spleen ferritin (HoSF) and an oxy-hydroxide-phosphate phase in plant and prokaryotic ferritins. The structure reflects a dynamic process of deposition and dissolution, influenced by different biological, chemical and physical variables. In this work we shed light on this matter by combining a structural (High Resolution Transmission Electron Microscopy (HRTEM) and Fe K-edge X-ray Absorption Spectroscopy (XAS)) and magnetic study of the mineral core biomineralized by horse spleen ferritin (HoSF) and three prokaryotic

ferritin-like proteins: bacterial ferritin (FtnA) and bacterioferritin (Bfr) from *Escherichia coli* and archaeal ferritin (PfFtn) from *Pyrococcus furiosus*. The prokaryotic ferritin-like proteins have been studied in native conditions and inside the cells for the sake of preserving their natural attributes. They share with HoSF a nanocrystalline structure rather than an amorphous one as has been frequently reported. However, the presence of phosphorus changes drastically the short-range order and magnetic response of the prokaryotic cores with respect to HoSF. The superparamagnetism observed in HoSF is absent in the prokaryotic proteins, which show a pure atomic-like paramagnetic behaviour attributed to the phosphorus breaking the Fe-Fe exchange interaction.

1 Introduction

Ferritin-like proteins are a family of complex cage proteins found in single cells organisms such as archaea and bacteria as well as multicellular organisms as plants and mammals. The physiological role of ferritin-like proteins is double: storing Fe, an essential nutrient, and protecting cells from potentially toxic effects of excess free Fe^{2+} (*1–6*).

They are formed by similar or identical subunits self-assembled into a hollow globular shell that contains an iron core consisting of a ferric oxy-hydroxide mineral similar to the nanomineral ferrihydrite (*7*). The biomineral core presents a high phosphate content (Fe:P $\approx$ 1:1) in bacteria and plants, whereas in mammals, the phosphate content is smaller (Fe:P $\approx$ 8:1) (*3*).

There are three types of ferritin-like proteins in prokaryotes: classical ferritins (Ftn), which are similar to eukaryotic ferritins, bacterioferritin (Bfr), and "DNA-binding proteins from starved cells" (Dps proteins). Ftn and Bfr are composed of 24 subunits, while Dps is a 12-meric protein. Ftn and Bfr show the same cage-like architecture of 12-13 nm diameter with a central cavity of 6-8 nm that essentially defines their function. The biomineral core that are reversibly

formed inside the protein cages, are heterogeneous in size and can vary from 1 to 4500 iron atoms/protein cage, depending upon cellular iron availability (*1, 7–9*).

The structure and magnetic properties of the inorganic core of eukaryotic proteins have been studied in several systems, including hepatic ferritin (*10*), native horse spleen ferritin (HoSF) (*11–13*), plants ferritin (*14*), mitochondrial ferritin in mouse (*15,16*) and drosophila (*17*) as well as in artificially loaded apoferritin under controlled conditions (*11, 18–20*). The generally accepted structure of the core is similar to that of inorganic ferrihydrite (*19, 20*). However, there is still debate about the structure of ferrihydrite itself, since this mineral appears only in nanoscale grains and presents long range disorder (*21, 22*). Two different ferrihydrite models have been proposed: Drits et al. (*23*) suggest a multiphase structure, while Michel and coworkers (*24, 25*) a single phase in which $\approx 90\%$ of the iron is octahedrally coordinated to oxygen and $\approx 10\%$ is tetrahedrally coordinated, with the tetrahedral iron surrounded by octahedral iron. Both, inorganic ferrihydrite and bioferrihydrite, present antiferromagnetic order at low temperature and hysteresis, due to uncompensated moments at the surface of the nanoparticles (*26–28*) or/and from the arrangement of magnetic moments at tetrahedral and octahedral Fe sites (*25*).

In contrast to eukaryotic ferritins, the structure and magnetic properties of prokaryotic ferritins has been much less studied. It is generally accepted that the core is composed of a Fe oxy-hydroxide-phosphate phase (*11, 29, 30*) less ordered than that of mammalian ferritins. The presence of phosphorus in the core should be a consequence of the higher phosphorus content of the cytoplasm of the prokaryotic cells in which the biomineralization takes place as compared to the much lower phosphorus content of the cytoplasm of the mammalian cells (*11, 31*).

The present work is focused on the structure and the magnetic properties of the mineral core synthesized by different ferritin-like proteins. With this aim, our approach towards unraveling the structure of the mineral core consists, on the one hand, of combining a structural analysis with a magnetic study, taking advantage of the close relationship between the magnetic

properties and the structure at the nanoscale, and on the other hand, of the comparison of the HoSF core with three native prokaryotic cores from: bacterial ferritin (FtnA) and bacterioferritin (Bfr) of *Escherichia coli* and archaeal ferritin (PfFtn) of *Pyrococcus furiosus*. The study of prokaryotic cores have been carried out in the whole cells, instead of purified proteins, in order to preserve their natural attributes.

The structure of the mineral cores has been studied by means of X-ray Absorption Spectroscopy (XAS) and High Resolution Transmission Electron Microscopy (HRTEM), and correlated with the magnetic response. Additionally, from the magnetic analysis we have been able to quantify the Fe storage capacity of the three prokaryotic ferritin-like proteins.

Knowing in detail the structure of the mineral core of ferritin-like proteins in native conditions is a key step towards understanding, among others, the reactivity of the protein or the mineralization process followed to generate the inorganic core. In fact, the mineral structure reflects a dynamic process of deposition and dissolution, influenced by the rate of ferritin biomineral formation, which depends in turns of other biological, chemical and physical variables. This knowledge will shed light on recently evolving fields related to the study of the implications of ferritin dysfunctions in neurodegenerative diseases (*32–36*), the use of the protein shell or apoferritin as a nanoreactor for synthesizing inorganic nanostructures (*37*), the role in the biomineralization process of magnetite by magnetactic bacteria (*52, 60*) or other applications in electronics (*38–40*), catalysis (*41*) and biomedicine (*42, 43*).

2 Materials and methods

2.1 Bacterial strains and growth conditions

Three recombinant *E. coli* strains that overexpress different prokaryotic ferritin-like proteins were used: i) *E. coli* DH5α harbouring plasmid pUC18A2(*ftnA, Ap*r) (*44*) that overproduces bacterial ferritin A (FtnA) ii) *E. coli* DH5α harbouring plasmid pGS281(*bfr, Ap*r) (*45*) that

overexpresses bacterioferritin (Bfr) iii) *E. coli* BL21 (DE3) harbouring a gene for ferritin from *Pyrococcus furiosus* cloned into pET-11a vector (*46*) that overproduces ferritin (PfFtn) from this hyperthermophilic archaeon. *E. coli* DH5α was used as unamplified control culture. Cultures were grown aerobically at 37 °C and 250 r.p.m. in Luria Bertani Broth (LB). In some batches LB was supplemented with 100 μM Fe(III)-citrate. In the case of the recombinant strains, the medium was supplement with 100 μg/ml ampicillin. *E. coli* DH5α(FtnA) and *E. coli* DH5α(Bfr) strains were grown to the stationary phase. *E. coli* BL21(PfFtn) was grown to OD_{600}=0.6 and gene expression was induced by addition on 0.5 mM IPTG and the culture was incubated further for 3-4 h. Cells were harvested by centrifugation at 5500 r.p.m. and 4 °C for 15 min. The pellets were washed tree times with PBS and finally stored at -20 °C. For XAFS and magnetic measurements, frozen cell pellets were lyophilized and then compacted into 4 mm diameter disks.

2.2 Gel electrophoresis

Protein expression was followed by polyacrylamide gel electrophoresis (PAGE) under sodium dodecyl sulphate denaturing (SDS-PAGE) and non-denaturing (Native- PAGE) conditions. The protein content in the samples was determined by the bicinchoninic acid (BCA) protein assay (Pierce) with bovine serum albumin as standard. Horse spleen ferritin (HoSF) purchased from Sigma-Aldrich was included. For SDS-PAGE frozen cells were thawed at 37 °C, suspended in 1mM dithiothreitol, 1mM phenylmethylsulfonyl fluoride, 1mg/ml of lysozyme and incubated in ice for 30 min. 15 μg protein samples were mixed with Laemmli buffer, heated at 95 °C for 5 min, then resolved by 15% SDS-polyacrylamide gel prior to staining with Coomassie Blue G-250. For Native-PAGE frozen cells were thawed at 37 °C, suspended in Tris-EDTA pH 8.0 with 10% of n-dodecyl β-D-maltoside and broken with a bead beater. The supernatant was incubated with 5U/μl Benzonase endonuclease for 30 min at room temperature. 70 μg protein samples

were mixed with sample buffer and then resolved by a pre-cast 4-16% NativePAGE Novex Bis-Tris Gel (Life Technologies). Iron staining was done with Prussian Blue: freshly made mixture (1:1, vol/vol) of 2% $K_4Fe(CN)_6$ and 2% HCl. Subsequently proteins were stained with Coomassie Blue G-250. Three replicated geles were run.

The percentage of ferritin-like proteins in the samples was estimated densitometrically on the stained gels (SDS and Native gels) using GeneTools analysis software v.4.02 (Syngene). The intensity of the selected bands was estimated and normalized to the total level of proteins calculated from each lane. Finally the relative density of the selected bands with respect to the corresponding bands from the control strain was calculated.

2.3 X-ray Absorption Spectroscopy (XAS)

The XAS experiment was performed at the ESRF synchrotron facility (France) in the BM23 beamline. All the spectra were measured at 70 K, with the storage ring working at low intensity, ≈80 mA, in 16 bunch mode. In this way, we avoid any damage to the biological sample. For non-overexpressing *E. coli* DH5α, the control sample, the spectra were measured at room temperature and multiple bunch mode. The spectra were recorded simultaneously in transmission and fluorescence geometries with a single-element silicon drift diode (SDD) detector and using a double crystal Si(111) monochromator. To improve the data reliability, between 3 and 5 spectra were recorded for each sample. The X-ray absorption spectrum of a Fe foil was measured using the transmitted intensity of the sample. In these conditions, the edge position of the sample can be determined with an accuracy of 0.2 eV. The normalized EXAFS functions, $\chi(k)$, were extracted from the raw data using a standard procedure. The absorption above the edge was extracted using a cubic spline in the k range $2 \leq k \leq 13$ Å^{-1} . The origin of the k space has been taken at the inflection point of the absorption edge. The Fourier transforms of $\chi(k)$ were performed in the k range $2 \leq k \leq 13$ Å^{-1} with a k^2 weight and a Hanning window

function.

2.4 Transmission Electron Microscopy (TEM)

Prokaryotic cells were fixed overnight in 2% glutaraldehyde in 0.1 M Sörenson phosphate buffer and washed in iso-osmolar phosphate/sucrose buffer. After repeated washing in distilled water, samples were dehydrated through an acetone series and embedded in Epon Polarbed resin in beem capsules, which polimerized at 55 °C for 48h. Ultrathin sections were obtained using a Diatome diamond knife in a Leica UCT ultramicrotome and deposited onto 300 mesh Holey Carbon Film. On the other hand, HoSF was deposited onto a 300-mesh carbon-coated grid. TEM images were taken at a PHILIPS CM120 at the University of Basque Country, working at 120 kV and High-resolution TEM (HRTEM) images, for selected samples, were taken at a TITAN3 (FEI) microscope at the Instituto de Nanociencia de Aragón (Spain), working at 300 kV. This Ultra High Resolution microscope is equipped with a SuperTwin objective lens and a CETCOR Cs-objective corrector from CEOS Company allowing a point to point resolution of 0.08 nm. Correction of the spherical aberration of the objective lens improves significantly the spatial resolution of the HRTEM images.

2.5 Magnetic characterization

For the magnetic analysis we used a sample holder consisting on a hole in the centre of a strip of paper where the pill was put in place. Magnetic measurements were performed in a SQUID magnetometer (Quantum Design, MPMS-7). Hysteresis loops were measured at 5 K and a maximum applied field of 6.5 T on two replicates. The evolution of the magnetization with temperature was measured by following a Zero-field cooling - field cooling (ZFC-FC) procedure: the sample is cooled from room temperature down to 5 K at zero applied magnetic field, then a magnetic field of 50 mT is applied and the magnetization is measured while heating

up to 300 K (ZFC). Without removing the field, the sample is cooled down to 5 K and the magnetization is measured as the temperature is risen up to 300 K (FC).

3 Results

3.1 Characterization of cultures

The expression of ferritin-like proteins has been followed by polyacrylamide gel electrophoresis (PAGE) under sodium dodecyl sulphate denaturing (SDS-PAGE) and non-denaturing (native-PAGE) conditions. SDS- PAGE was used to estimate the relative molecular mass of the apoprotein subunits and their relative abundance in the cells. The ionic detergent SDS denatures the proteins to the linear shape, removing any higher order structure. A native gel was run to determine whether the overexpressed ferritin proteins assemble into a large complex that can store iron.

SDS-gel electrophoresis of the three recombinant strains together with a control batch of *E. coli* and the horse spleen ferritin (HoSF) is shown in figure 1. The band corresponding to HoSF is around 20 kDa and all overexpressing strains show high density bands of approximately the same molecular weight. However, significantly dense bands around 20kDa are not seen in the control strain. As expected, no differences, in the molecular mass, are observed in the batches cultivated with or without supplemented Fe. The estimated FtnA and Bfr contents, obtained in the densitometry analysis, represent approximately 12% of the total protein in the lanes, and no differences were found between cells grown in Fe supplemented and non-supplemented media. In the case of PtFtn, the estimated content ranged from 6% in cells grown in non-supplemented medium to 20% in cells grown in Fe-supplemented medium.

The native gel was stained both with Prussian blue for iron and Coomassie for proteins (figure 2). Protein staining reveals the four prokaryotic samples with an electrophoretic mobility similar to the horse spleen ferritin used as marker. Very high dense bands can be seen in the

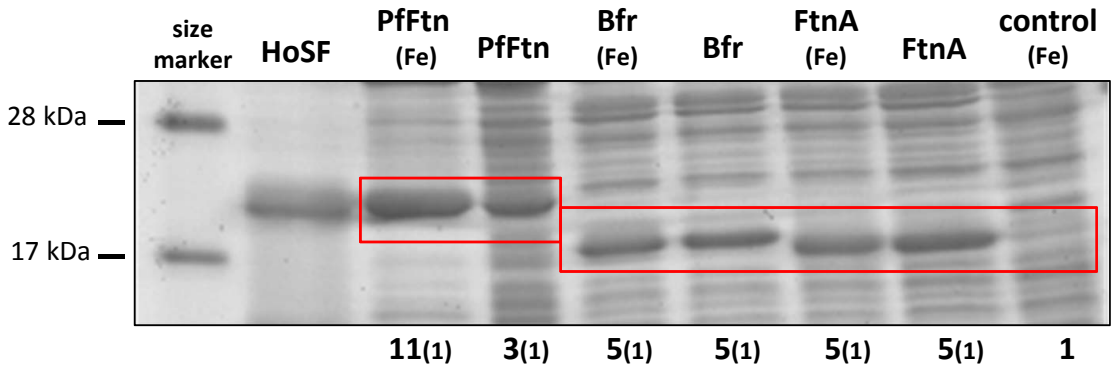

Figure 1: SDS gel stained with Coomassie G-250 for horse spleen ferritin (HoSF); *E. coli* overexpressing archaeal ferritin (PfFtn), bacterioferritin (Bfr) and bacterial ferritin (FtnA) and non-overexpressing *E. coli* DH5α (control).The strains were grown in non-supplemented and iron supplemented medium (named Fe). The relative density of the selected bands with respect to the control is indicated at the bottom of the gel.

lanes of the three recombinant strains. Iron staining shows very light characteristic-blue bands in all cells extracts in coincident positions with bright bands appearing in Coomassie staining, which indicates that the subunits have assembled into a functional protein that binds iron. The percentage of ferritin-like proteins in the samples was estimated by densitometry in the native gel stained with Coomassi. The results are similar to that obtained from SDS gel. In the control strain, the estimated FtnA and Bfr contents represent around 3% of the total protein in the lane. This means that the FtnA:Bfr ratio is 1:1 in the non-overexpressing control strain. In the recombinant strains, the band corresponding to the overexpressed protein appears markedly intensified. This selected band represents 16% of the total protein in the lane in the case of the FtnA and Bfr overexpressing strains, and up to 25% in the PfFtn overexpressing strain. This situation obviously unbalances the ratio between ferritin-like proteins in the cell. We found difficulties to calculate this rate in the overexpressed strains because the band corresponding to the overexpressed protein overlaps the other ferritin like-protein bands in some of the lanes. Finally, we estimated a ratio by comparing the intensity of the selected band in each lane with

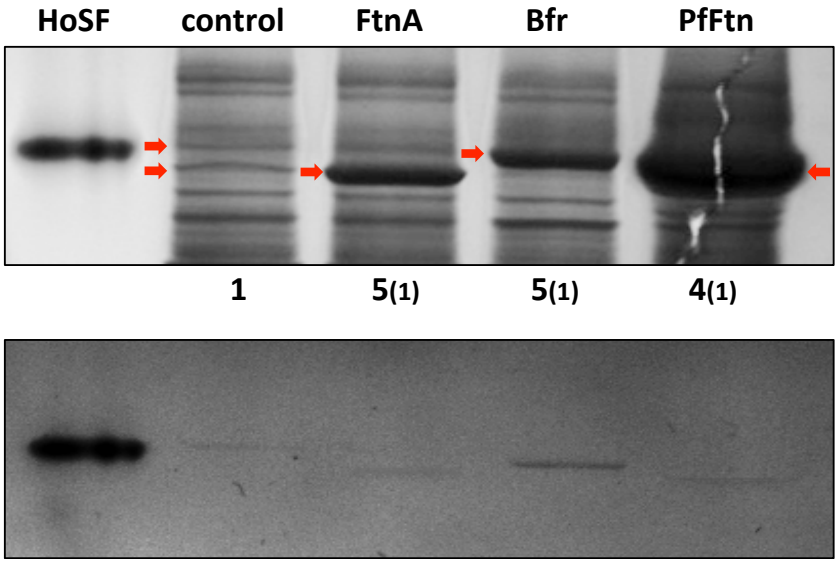

Figure 2: Native gel stained with Coomassie G-250 (upper four lanes) and Prussian blue (lower four lanes) for horse spleen ferritin (HoSF); non-overexpressing *E. coli* DH5α (control); *E. coli* overexpressing bacterial ferritin (FtnA), bacterioferritin (Bfr) and archaeal ferritin (PfFtn). The relative density of the selected bands with respect to the control is indicated at the bottom of Coomassi gel. The arrows mark the selected bands. All strains were grown in iron supplemented medium.

those corresponding in the control lane giving a FtnA/Bfr ratio of ≈1:5 and ≈5:1 for FtnA and Bfr overexpressing strains, respectively. In the case of the PfFtn overexpressing strain, the ratio of interest PfFtn/(Bfr+FtnA) is ≈4:1.

3.2 Magnetic measurements

In Figure 3 we show the dependence of the magnetization with the applied magnetic field, $M(H)$, and with temperature, $M(T)$, for the prokaryotic samples and HoSF. In the case of the prokaryotic cells, we have been working with the batches cultured with and without supplemented Fe. The thermal evolution of the magnetization was performed by means of a zero-field cooling, ZFC, and field cooling, FC, procedure. This means that the sample was cooled at low temperature without applied magnetic field (ZFC) or with magnetic field (FC) and then the magnetization was measured while increasing temperature under an applied magnetic field of

50 mT.

As shown in Figure 3, important differences are detected in the magnetization behavior for the HoSF and the prokaryotic ferritin-like proteins. HoSF displays a superparamagnetic behaviour identified by the appearance of a maximum in the ZFC magnetization curve at a blocking temperature, $T_B \approx 15$ K, in agreement with the literature (*26*). At the same time, the hysteresis loops of HoSF display remanence and coercivity below T_B but are anhysteretic at higher temperatures, $T > T_B$. As reported previously, the superparamagnetic behaviour found in the cores of mammalian ferritin (*26*) and inorganically synthesized ferrihydrite (*47*) is due to uncompensated moments at the surface of the antiferromagnetic ferrihydrite core (*26–28*). On the contrary, in the case of the prokaryotic samples, as shown in Figure 3, the ZFC-FC measurements at 50 mT display an unblocked and reversible evolution of the magnetization in the whole temperature range studied (5-300 K). In the same way, the magnetization versus field measurements $M(H)$ exhibit an anhysteretic Langevin-like behaviour at 5 K and a linear behaviour at T$\geq$ 20K (not shown). These results indicate that the mineral core synthesized by the prokaryotic ferritin-like proteins lacks magnetic order and behaves like a paramagnet.

Quantitative values of the magnetic moment per core have been obtained by fitting the magnetic data to the following expression:

$$M = M_0 \mathcal{L}\Big(\frac{\mu\mu_0 H}{k_B T}\Big) + \chi H = M_0 \Big[\coth\Big(\frac{\mu\mu_0 H}{k_B T}\Big) - \frac{k_B T}{\mu\mu_0 H}\Big] + \chi H \qquad (1)$$

Here, $\mathcal{L}$ is the Langevin function, M_0 is the saturation magnetization, μ is the magnetic moment per protein core, μ_0 is the vacuum permeability. χ is a susceptibility term that accounts for the linear behaviour from the diamagnetic signal of the organic components, the sample holder and the antiferromagnetic signal from the ferrihydrite core, in the case of HoSF. In fact, the susceptibility χ has been found to be temperature dependent (*26*) for HoSF, but in the case of the prokaryotic cells, χ is a small contribution compared to the first term of equation 1,

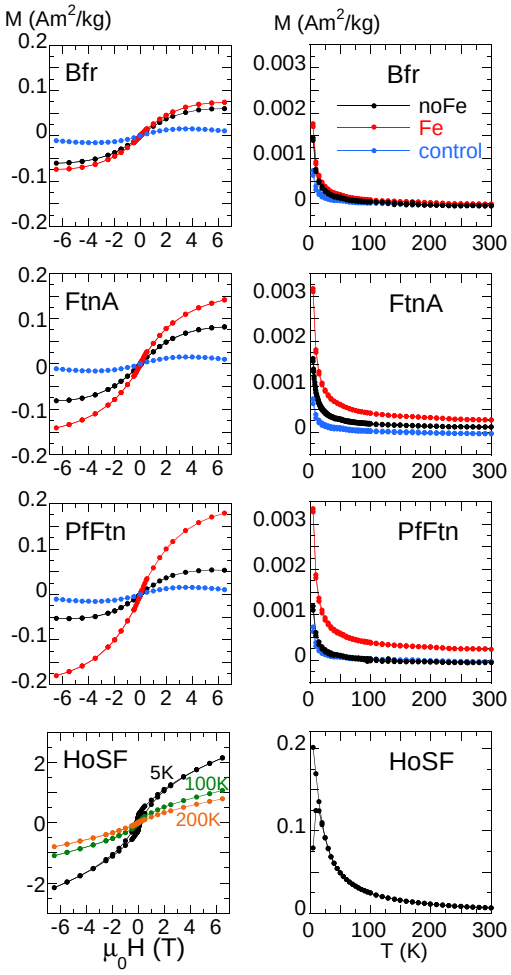

Figure 3: 5 K hysteresis loops (left) and 50 mT ZFC-FC curves (right) of *E. coli* overexpressing bacterioferritin (Bfr), bacterial ferritin (FtnA) and archaeal ferritin (PfFtn) for the batches with and without supplemented Fe (named 'Fe' and 'noFe', respectively). The wild-type *E. coli* DH5α grown in Fe supplemented medium (control) is also shown. The lowest panel displays the 5, 100 and 200K hysteresis loops (left) and 50 mT ZFC-FC curve of horse spleen ferritin (HoSF).

and temperature independent. We have fitted simultaneously the $M(H)$ and $M(T)$ of each prokaryotic samples. This way, only three parameters were left free: μ, M_0 and χ, and were common for the $M(H)$ and $M(T)$ fits. An example of the fit is shown in the SI.

Results for the HoSF give a magnetic moment per core of $\approx$ 340 μ_B, in agreement with the literature, where values between 113 and 550 μ_B have been found (*48*). Regarding the prokaryotic samples, the most striking result obtained from the magnetic fits is the very low magnetic moment per particle core, ranging between 6 and 8 μ_B. This is much lower than the value obtained for HoSF ($\approx$ 340 μ_B). Basically, 6-8 μ_B is an atomic-like magnetic moment (Fe^{3+} should contribute with 5 μ_B), which indicates that we have a paramagnet from individual uncoupled Fe^{3+} ions. In fact, this point has been confirmed by the fact that the magnetic data follow nicely a Brillouin function corresponding to an atomic paramagnet with an Fe^{3+} magnetic moment (see SI).

From M_0, obtained from the fit of $M(H)$ and $M(T)$, we can estimate the amount of Fe^{3+} ions stored in the cell. This is because $M_0 = N\mu$, where N is the number of Fe^{3+} ions per gram (dry weight) and μ is the magnetic moment of Fe^{3+}. This estimation is presented in Figure 4.

We can observe that, the amount of iron is approximately the same in the three overexpressing *E. coli* strains ($\approx$ 1.65x10^{18} Fe^{3+}/g) and $\approx$ 75-90% higher than the non overexpressing control strain, when cells are grown in iron non supplemented medium.

In Fe supplemented medium the amount of Fe^{3+} ions stored in the cells increases, but this increment is different depending on the strain. For the wild-type *E. coli* the Fe^{3+} ions stored increase $\approx$ 45%. For the overexpressing strains we found an increment of $\approx$ 140% for archaeal ferritin (PfFtn), $\approx$ 40% for bacterial ferritin (FtnA) and $\approx$ 13% for bacterioferritin (Bfr). The huge increment of Fe^{3+} ions stored in PfFtn could be explained from the densitometry analysis that estimates a three-fold increment of the overexpressed protein with respect to the control. Unfortunately, we cannot estimate the amount of Fe^{3+} ions per core but through the magnetic

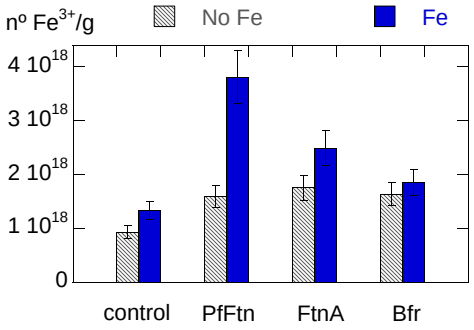

Figure 4: Number of Fe^{3+} ions per gram of cells (dry weight) in *E. coli* overexpressing archaeal (PfFtn), bacterial ferritin (FtnA) and bacterioferritin (Bfr), grown with and without supplemented Fe (named Fe and noFe, respectively). The wild-type *E. coli* is also shown as control.

analysis we clearly infer that both overexpression and the addition of Fe in the medium give rise to an increment of the amount of Fe^{3+} ions stored in the cells.

3.3 Fe K-edge X-ray Absorption Spectroscopy (XAS)

XAS, unlike conventional diffraction methods, does not require long range order, and, due to its local structure sensitivity and excellent spatial resolution is an excellent tool for studying both atomic and electronic structure of nanoparticles, with independence on the core size of the proteins. In fact, the XAS spectra of the wild-type *E.coli* DH5α grown in non-supplemented and iron supplemented media are similar, figure 2S in supplementary information (SI), even though a different repletion is expected in each case.

X-ray Absorption Near Edge Structure (XANES) provides electronic and structural information around the absorbing atom by fingerprinting with the spectrum of a reference compound. Several characteristic features can be distinguished in the XANES region: i) the edge position can be used to assign the oxidation state of the absorber; ii) the pre-edge structure depends on the nature and the symmetry of the absorber, and iii) the post-edge region gives information of the medium range order around the absorbing atom.

Figure 5 shows the Fe K-edge XANES spectra of the biological samples (control, Bfr, FtnA,

PfFtn and HoSF) together with inorganic 6-line ferrihydrite synthesized at the laboratory following the recipe in (*49*). All the studied samples present the same edge position, coincident with that of the inorganic ferrihydrite, a clear indication of the Fe ions being Fe^{3+}. On the other hand, the XANES of the three prokaryotic samples are identical but present some differences with respect to HoSF, the latter being closer to inorganic ferrihydrite.

Firstly, the pre-edge peak of the prokaryotic samples shows a double structure whereas HoSF and inorganic ferrihydrite display a single peak with higher amplitude. As it is well known, the intensity of the pre-edge peak is smaller for Fe^{3+} octahedral compounds, with centrosymmetric sites, than for Fe^{3+} tetrahedral compounds (*50*). In the present case, the area of the ferrihydrite and HoSF samples is 0.12-0.13, similar to that reported for other ferrihydrites (*50*), while for the prokaryotic samples the area is lower, close to 0.08, which suggests a more centrosymmetric environment. Other differences lie in the structure above the edge. In all prokaryotic samples there is a shoulder at ≈ 7137 eV that is not present in HoSF or inorganic ferrihydrite. This shoulder has been also observed in $FePO_4 \cdot 2H_2O$ (*50*), in poorly ordered ferric phosphates (*51, 52*) and it has been related to the presence of phosphorus in the surrounding of the Fe atoms. We will discuss this matter later on in the EXAFS analysis.

The extended region of the spectra (Extended X-ray Absorption Fine Structure, EXAFS), $\chi(k)$, contains structural information of the first atomic shells around the absorbing Fe atom. The normalized $\chi(k)$, Figure 6, were extracted from the raw data using the standard procedure (*53*) for electron momentum up to $k = 13$ Å^{-1}. In order to obtain direct space information, a Fourier transform of $\chi(k)$, $\Phi(R)$, is performed for the k range $2.5 \leq k \leq 13$ Å^{-1} to obtain a pseudo-radial distribution function of atoms around the absorber. $\Phi(R)$ presents two major peaks. The first peak, at $R = 1.5$ Å corresponds to the O nearest neighbors around the absorbing Fe atom. The second peak, at $R = 2.6$ Å corresponds mainly to neighboring Fe atoms. Note that the first peak is much higher than the second. No further peaks are detected at higher

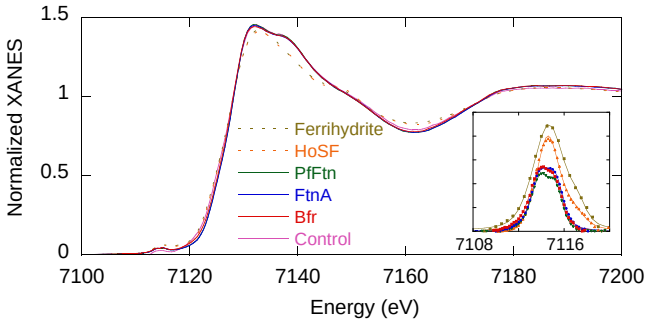

Figure 5: XANES spectra of ferrihydrite synthesized inorganically, horse spleen ferritin (HoSF), *E. coli* DH5α (control), and *E. coli* overexpressing bacterial ferritin (FtnA), bacterioferritin (Bfr) and archaeal ferritin (PfFtn) for the batches with supplemented Fe. The inset shows a detail of the pre-edge peaks. All spectra were measured at 70K except the control that was measured at room temperature.

distances, a sign of a lack of long range order in all the samples studied.

There are two remarkable differences between the $\Phi(R)$ of the prokaryotic and HoSF cores: i) the main peak, corresponding to the Fe-O shell, is much higher in the prokaryotic ferritins than in HoSF; ii) in HoSF, the peak at 2.6 Å presents a double structure absent in the prokaryotic samples.

To get quantitative information about the local structure around the Fe atoms, the Fourier transform of the two main peaks ($0.5 \leq R \leq 3$ Å) was fitted to the well-known EXAFS function (see SI) as the sum of spherical coordination shells with gaussian distribution of atoms, having average coordination number N at a distance R, and variance σ^2. The latter gives a mean square relative displacement between the absorber and the scatter pairs, also known as the Debye-Waller factor. Details of the data analysis can be found in the SI. Two different approaches have been used for the fitting. In the case of HoSF we have considered a three-shell model: one Fe-O coordination shell and two Fe-Fe coordination shells, the latter is justified by the double structure observed in the second peak of the Fourier transform $\Phi(R)$.

As a first approximation, we have used a two-shell model for the prokaryotic samples, one for Fe-O and one Fe-Fe atoms, but the fit improves with an additional Fe-P coordination shell,

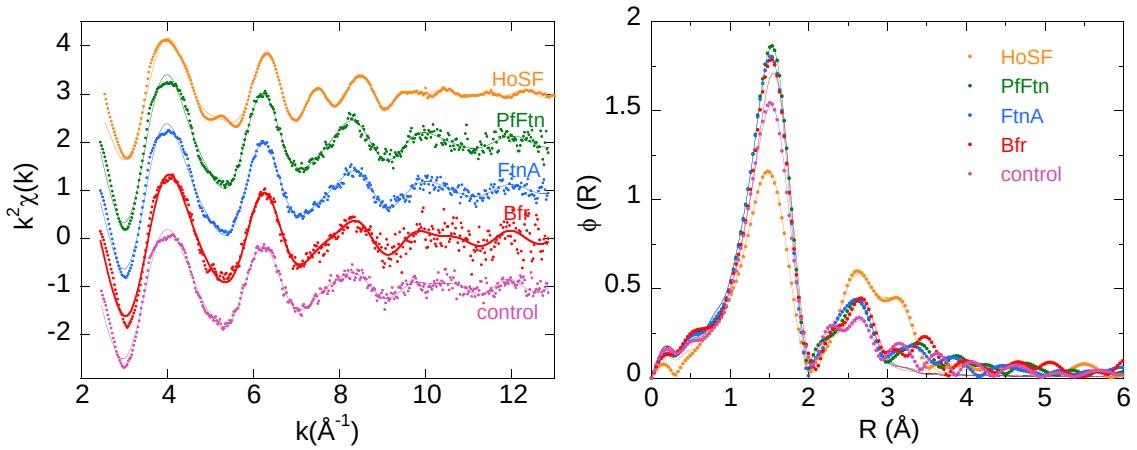

Figure 6: Left: EXAFS spectra of horse spleen ferritin (HoSF) and *E. coli* overexpressing archaeal ferritin (PfFtn), bacterial ferritin (FtnA) and bacterioferritin (Bfr) for the batches with supplemented Fe. Right: Fourier transform of $\chi(k)$. The corresponding fits to the experimental data (lines) are also plotted in both $k-$ and $R-$ spaces. All spectra were measured at 70K except for the control that was measured at room temperature.

as suggested by XANES spectroscopy.

The interatomic distances R, coordination numbers N, and Debye-Waller factors σ^2 obtained for each shell are shown in Table 1. The quality of the fits measured by the S^2 factor (see definition in the SI) is given in Table 1 and can also be checked in Figure 6. Note that in Figure 6, the fit in $k-$ space is shown together with the full experimental spectra, and not with the filtered spectra obtained from the back-Fourier transform of the two main peaks ($0.5 \leq R \leq 3$ Å). The fact that the fit of the first two peaks follows nicely all the EXAFS oscillations is a confirmation of the lack of long range order. Attempts to refine the experimental data assuming an amorphous environment around the absorbing atom were also made (see SI). However, this led to unsatisfactory fits, indicating that the lack of long range order is not due to a completely amorphous structure, but rather to the fact that the mineral core consists of nanosize particles, as will be further discussed.

In the prokaryotic samples, we obtain ≈ 6 O at 2.0 Å in the first coordination shell and an Fe-Fe shell at 3.0 Å with a coordination number that ranges from 2 for control and Bfr to 3

for FtnA and PfFtn. There is also an additional Fe-P coordination shell at 2.65 Å with a low number of phosphorus ranging from 0.4 for control and BFr to 0.8 for FtnA and PfFtn. These findings reflect a ratio Fe:P of $\approx$ 4:1 for the prokaryotic ferritin-like proteins grown in native conditions, higher than the one reported in reference (*11*).

Finally, the Debye-Waller factor, σ^2, has a small temperature contribution because the spectra were recorded at 70 K, except for the control sample that was measured at room temperature, and we do not find appreciable difference between them. Thus, their values are ascribed mainly to the degree of structural disorder. The most remarkable result is that the HoSF reaches a Debye-Waller factor for the Fe-O shell that is twice that of prokaryotic samples, as clearly reflected in the strong reduction of the first peak of $\Phi(R)$, already pointed out (Figure 6b). The larger disorder, together with the shorter distance and the lower coordination number found in Fe-O for the HoSF as compared to the prokaryotic samples could be attributed to the presence of some Fe-O in a tetrahedral environment as proposed by Michel et al. (*24*) for inorganically synthesized ferrihydrite. Also, the analysis of the pre-edge peak of the XANES spectra suggested a more disordered environment for HoSF than for the prokaryotic ferritin-like proteins, which present a Fe-O shell with lower disorder and an interatomic distance and coordination number that corresponds to a pure octahedral environment ($R_{Fe-O} = 2.00$ Å, $N_{Fe-O} = 6$).

3.4 High Resolution Transmission Electron Microscopy (HRTEM)

Figure 7 shows the images of the bacterial ferritin (FtnA), bacterioferritin (Bfr) and the horse spleen ferritin (HoSF) together with the Fourier transform of marked nanoparticles and the size histograms. All nanoparticles present spherical shapes with mean size diameter ranging from $\approx$ 3 to 4 nm being higher the size on the HoSF. Several particles show one or two sets of well-defined lattice fringes. The Fourier transform of selected areas reveals four lattice spacings, different for the HoSF and the prokaryotic ferritin-like proteins. The lattice spacing distributions

Table 1: N, coordination number; R(Å), interatomic distance; σ^2(Å^2), Debye-Waller factor as obtained from the fit analysis of the EXAFS spectra of the studied samples: horse spleen ferritin (HoSF), *E. coli* DH5α (control) and *E. coli* overexpressing bacterioferritin (Bfr), bacterial ferritin (FtnA) and archaeal ferritin (PfFtn). All the strains were grown in Fe supplemented medium. S^2 represents the goodness of the fit.

	Control	Bfr	FtnA	PfFtn	HoSF
N_{Fe-O}	5.7 (2)	5.9 (2)	5.9 (2)	6.0(2)	5.5(2)
R_{Fe-O} (Å)	2.00(1)	2.00(1)	1.99(1)	2.00(1)	1.98(1)
σ^2_{Fe-O}(Å^2)	0.009 (1)	0.007(1)	0.006(1)	0.006(1)	0.011(2)
N_{Fe-P}	0.4 (2)	0.4(2)	0.8(4)	0.8(2)	-
R_{Fe-P} (Å)	2.68(4)	2.66(5)	2.64(5)	2.65(6)	-
σ^2_{Fe-P}(Å^2)	0.004 (3)	0.005(4)	0.015(8)	0.009(5)	-
N_{Fe-Fe}	2.1(1)	2.0(2)	3.2(5)	2.7(4)	2.7(3)
R_{Fe-Fe} (Å)	3.03(2)	3.04(2)	3.03(2)	3.03(2)	3.00(2)
σ^2_{Fe-Fe}(Å^2)	0.013(3)	0.010(3)	0.008(3)	0.013(2)	0.011(1)
N_{Fe-Fe}	-	-	-	-	1.5(2)
R_{Fe-Fe} (Å)	-	-	-	-	3.45(1)
σ^2_{Fe-Fe}(Å^2)	-	-	-	-	0.005(1)
S^2	0.04	0.0604	0.0344	0.0365	0.0376

found for the mineral core of the prokaryotic ferritin-like proteins are similar between them but completely different to that found for HoSF as shown in Figure 7. Even though we cannot assign a particular core to a given protein, we must remember that the overexpressing strains present at least 5 times more ferritin-like protein than the wild-type strain.

In the case of HoSF, the Fourier transform can be well ascribed to the simulated patterns obtained from different ferrihydrite models (*23, 24*), see Figure 4S in the SI. On the contrary, for the prokaryotic ferritin-like proteins, the main lattice spacing is found at $\approx$ 2.9 Å and in some cores two systems of fringes at $\approx$ 2.9 Å and $\approx$ 2.6 Å can also be detected. For these particles, the lattice spacings and angular relationships found in the Fourier transform do not match with those models proposed for the ferrihydrite (*23, 24*). In order to discard the transformation of the mineral cores under the electron beam, the magnetite, hematite, maghemite and wüstite lattice spacings and angular relationships were compared against the obtained experimentally, but no

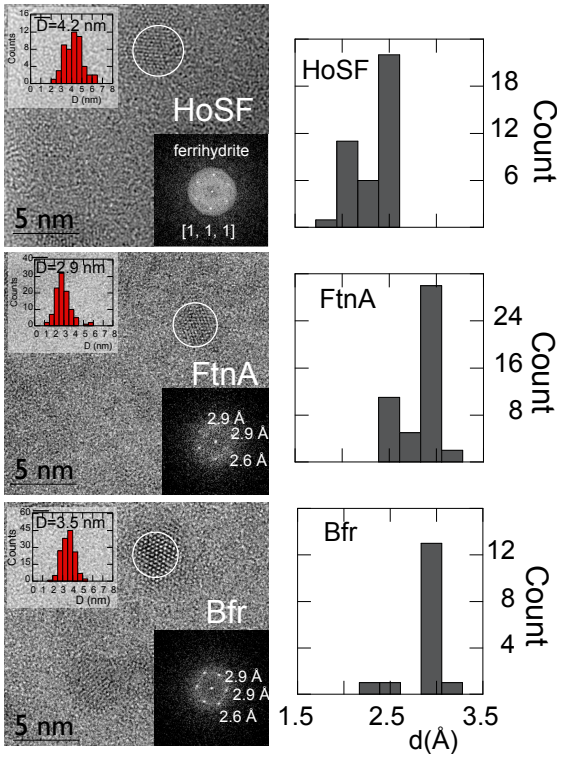

Figure 7: Left: HRTEM images, Fourier transforms of marked nanoparticles and size histograms, Right: Lattice spacing frequency of horse spleen ferritin (HoSF) and *E. coli* overexpressing bacterial ferritin (FtnA) and bacterioferritin (Bfr).

correlation between them was found.

4 Discussion

The structure and magnetic properties of three native prokaryotic ferritin-like proteins, bacterial ferritin (FtnA) and bacterioferritin (Bfr) of *Escherichia coli* and archaeal ferritin (PfFtn) of *Pyrococcus furiosus*, have been analyzed and compared to the eukaryotic horse spleen ferritin (HoSF). The prokaryotic cores have been studied inside the whole cells for the sake of preserving their natural attributes.

The percentage of ferritin-like proteins present in the prokaryotic cells as estimated by densitometry shows that in the wild-type *E. coli* strain (control) the FtnA:Bfr ratio is ≈1:1. In the

recombinant strains this ratio changes, being predominant the overexpressed protein by a factor of 5. The number of Fe^{3+} ions stored in the cells was estimated by means of a magnetic analysis and both overexpression and the addition of Fe in the culture medium give rise to an increment of the amount of Fe^{3+} ions stored in the cells. These findings are represented schematically in Figure 8 and must be taken into account when discussing the magnetic response and the structure of the mineral cores of the prokaryotic ferritin-like proteins. Even though, we are working with the whole cells, the major response, in all the techniques used, would come from the overexpressed ferritin-like proteins.

As shown by XAS spectroscopy, the ferritin-like protein cores of the three recombinant prokaryotic cells present the same structure. The structure consists in one Fe-O shell at R_{Fe-O}=2.0 Å, one Fe-P shell at R_{Fe-P}=2.65 Å and one Fe-Fe at R_{Fe-Fe}=3.03 Å. We should point out that even though the interatomic distance of the Fe-O is similar to those found in the literature (*11, 31*), the Fe-Fe and Fe-P interatomic distances differ with respect to previous works on isolated *Azotobacter vinelandii* bacterioferritin (*11*) and native Dps-like protein from *Streptococcus suis* (*31*), where the iron was found at ≈ 3.5 Å and the phosphorus at ≈ 3.2 Å. However, a similar structure has been found in plant ferritin from pea seed (*Fisum sativum L.*) with a Fe-Fe interatomic distance at 3.08 Å (*14*). Interestingly, ferritins in plants are located in plastids, that would have arisen by endosymbiosis of an ancient prokaryotic cell.

The results obtained for HoSF are similar to those found in the literature (*11–13*) with ≈ 5.5 O atoms in the first coordination shell, and a double Fe coordination shell at 3.0 Å and 3.45 Å with average coordination numbers of 2.7 and 1.5, respectively. These results are very similar to those found for inorganic ferrihydrite (*51, 52, 54–56*), with an Fe-O path at ≈ 1.98 Å and two Fe-Fe paths at ≈ 3.05 Å and ≈ 3.44 Å except for some differences in the average coordination numbers, specially for the outer Fe-Fe shells. However, we must take into account that the average coordination number is strongly dependent on the size of the nanoparticle (*57, 58*),

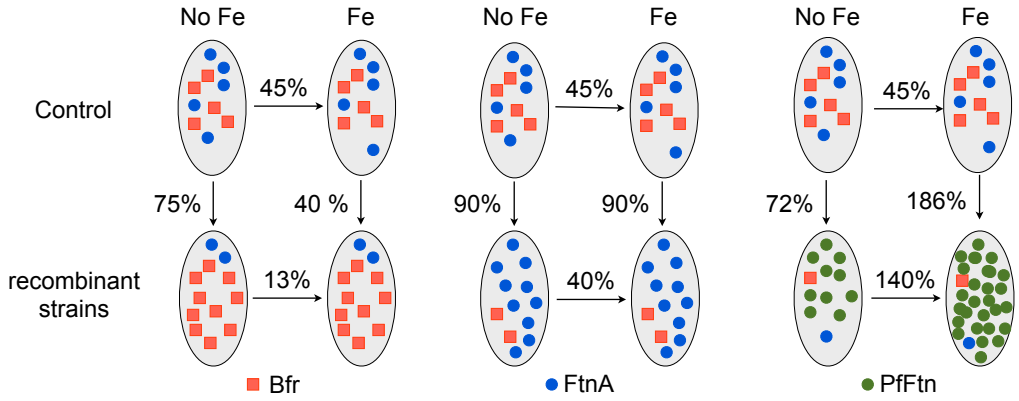

Figure 8: A simplified representation of the ferritin-like proteins presented in the wild-type *E.coli* (control) and the recombinant strains overproducing bacterioferritin (Bfr), bacterial ferritin (FtnA) and archaeal ferritin (PfFtn). Cells grown in non-supplemented (noFe) and supplemented (Fe) medium are drawn. The percentages correspond to the increment of Fe^{3+} ions registered by comparing the different batches obtained from the magnetic analysis.

because surface Fe atoms are undercoordinated and when decreasing the nanoparticle size, the number of surface-to-volume atoms increases and as a consequence the average coordination number, detected by EXAFS, decreases.

Even though the structure of the core biomineralized by the three prokaryotic proteins is similar, it differs clearly from that of HoSF, as highlighted by EXAFS and XANES spectroscopies. One remarkable difference is related to the oxygen coordination shell. In the case of the prokaryotic ferritin-like proteins, Fe presents an octahedral coordination, with 6 oxygen atoms at a distance of 2.0 Å and low mean structural disorder, σ^2 = 0.006 Å^2, independent of the strain studied. The high symmetry of the oxygen sites is also reflected in the pre-edge of the XANES spectra, with a double structure and low integrated area. This is not the case of HoSF, whose structural disorder, σ^2 = 0.011 Å^2, almost doubles that of prokaryotic proteins, and, at the same time, the integrated area of the pre-edge increases, an indication of the symmetry of the oxygen sites decreasing. All these issues suggest that in the HoSF tetrahedral and octahedral sites coexist, as it has been recently suggested for inorganically synthesized ferrihydrite (*24,59*).

Another aspect to discuss is the presence of phosphorus in the surroundings of the Fe atoms forming the mineral core. In the present work, we have not found phosphorus in the native core of HoSF, but our XAS measurements suggest that phosphorus is present in the native core of the three prokaryotic ferritin-like proteins analyzed. The presence of phosphorus in the structure of the mineral core of ferritins has been previously investigated in HoSF (*11*) and in Dps-like protein from *Streptococcus suis* (*31*). In those works, the structure of the mineral core was studied by means of EXAFS spectroscopy, both in native proteins and reconstituted in media with different Fe:P ratio contents. In the case of native HoSF, the local order structure found around the Fe atom was that of ferrihydrite (*51, 52, 54, 56*), similarly to what we have found in the present work and coincident with other works on HoSF (*11–13*). However, when HoSF is reconstituted in a phosphorus-rich medium, the structure changes, appearing a Fe-P coordination shell at 3.17 Å and only one Fe-Fe shell at 3.5 Å (*11*). On the other hand, the structure of the mineral core of native Dps-like protein, with a Fe-P shell at 3.2 Å and one Fe-Fe shell at 3.52 Å (*31*), changes markedly when the proteins are reconstituted in a phosphorus-free medium. In this case, the Dps-like protein biomineralizes a core similar to ferrihydrite, without phosphorus but with two Fe-Fe shells at 3.07 Å and 3.41 Å. Those results indicate that the final structure of the mineral core depends on the phosphorus content of the medium in which the biomineralization takes place, but not on the apoprotein cage itself. The recurrent presence of phosphorus observed in our native prokaryotic mineral cores could be thus attributed to the high phosphate content of the prokaryotic cytoplasm as compared to the mammalian cells. Interestingly, the presence of iron phosphate nanoparticles has also been reported in mitochondria linked to some human diseases such as Friedreich ataxia (*36*) and in the cytoplasm of magnetotactic bacteria during the biomineralization of magnetite nanoparticles (*52, 60*).

As shown, the structure of the prokaryotic mineral cores and the HoSF display remarkable

differences, but they also share some similarities, among which stand out their spherical shape their spherical shape and the lack of medium/long range order. As corroborated by HRTEM and EXAFS, the cores lack medium/long range order because of their nanometric size, but they are not amorphous as they exhibit clear short-range crystalline order.

Finally, regarding the magnetic properties of the protein cores, while HoSF cores retain an antiferromagnetic order, the prokaryotic ferritins are purely paramagnetic. The loss of the antiferromagnetic order observed in the prokaryotic ferritins can be explained in the light of the structural results. Because both prokaryotic and HoSF cores are crystalline, the loss of magnetic order can not be attributed to structural disorder but rather to a weakness of the Fe-Fe exchange interaction due to the presence of phosphorus atoms (*61*).

5 Conclusion

We have studied the structure and the magnetic response of prokaryotic (bacterial ferritin, archaeal ferritin and bacterioferritin) ferritin-like proteins, in native conditions, and compared the results with the horse spleen ferritin. All proteins biomineralize spherical crystal nanoparticles. The structural and magnetic properties of the three prokaryotic ferritin-like proteins studied are very similar, but differ remarkably from HoSF. One important difference is the local symmetry around the Fe, being octahedral for the prokaryotic cores and with higher disorder in the case of the HoSF which suggest a coexistence of octahedral and tetrahedral environment around the Fe. Another remarkable difference is the presence of phosphorus in the prokaryotic cores, absent in HoSF. The presence of phosphorus changes the short-range structural order around the Fe atoms in prokaryotic cores to a Fe oxy-hydroxide phosphorus rich phase different from the ferrihydrite-like structure observed in HoSF. The presence of phosphorus does also explain the breakdown of magnetic order observed in the prokaryotic cores, attributed to a weakening of the Fe-Fe exchange interaction.

Acknowledgements

We acknowledge Prof. J.M. Barandiarán for a critical reading of the manuscript. We are very grateful to Dr. Pierpaolo Ceci for his kind gift of the *E. coli* BL21(PfFtn) strain, and to Prof. Simon C. Andrews for providing us with the plasmids pUC18A2 and pGS281. We also thank Dr. R. Andrade and Dr. A. Ibarra for the TEM and HRTEM imaging, respectively, and I. Fernández for sample preparation for TEM. Part of the measurements were performed at the SGIker service of the University of the Basque Country (UPV/EHU). The Basque and Spanish Governments are acknowledged for funding under projects number S-PE11UN031 and MAT2014-55049-C2-1-R, respectively. Dr. J. Alonso acknowledges the financial support provided through a postdoctoral fellowship from Basque Government.

References

1. E. C. Theil, "Ferritin: Structure, gene regulation, and cellular function in animals, plants, and microorganisms," *Annu. Rev. Biochem.*, vol. 56, no. 1, pp. 289–315, 1987.

2. J. L. Smith, "The physiological role of ferritin-like compounds in bacteria.," *Crit. Rev. Microbiol.*, vol. 30, no. 3, pp. 173–85, 2004.

3. E. Theil, "Ferritin: the protein nanocage and iron biomineral in health and in disease," *Inorganic chemistry*, vol. 52, no. 21, pp. 12223–12233, 2013.

4. E. C. Theil, R. K. Behera, and T. Tosha, "Ferritins for chemistry and for life," *Coordination Chemistry Reviews*, vol. 257, no. 2, pp. 579 – 586, 2013.

5. P. Arosio, R. Ingrassia, and P. Cavadini, "Ferritins: A family of molecules for iron storage, antioxidation and more," *BBA - General Subjects*, vol. 1790, no. 7, pp. 589–599, 2009.

6. N. E. Le Brun, A. Crow, M. E. P. Murphy, a. G. Mauk, and G. R. Moore, "Iron core mineralisation in prokaryotic ferritins.," *Biochim. Biophys. Acta*, vol. 1800, no. 8, pp. 732–44, 2010.

7. L. Bevers and E. C. Theil, "Maxi- and Mini-Ferritins: Minerals and Protein Nanocages," *Prog. Mol. Subcell. Biol.*, vol. 52, pp. 29–47, 2011.

8. P. M. Harrison and P. Arosio, "The ferritins: molecular properties, iron storage function and cellular regulation," *Biochim. Biophys. Acta*, vol. 1275, no. 3, pp. 161 – 203, 1996.

9. A. J. Hudson, S. C. Andrews, C. Hawkins, J. M. Williams, M. Izuhara, F. C. Meldrum, S. Mann, P. M. Harrison, and J. R. Guest, "Overproduction, purification and characterization of the *Escherichia coli* ferritin," *Eur. J. Biochem.*, vol. 218, no. 3, pp. 985–995, 1993.

10. Y.-H. Pan, K. Sader, J. Powell, A. Bleloch, M. Gass, J. Trinick, A. Warley, A. Li, R. Brydson, and A. Brown, "3d morphology of the human hepatic ferritin mineral core: New evidence for a subunit structure revealed by single particle analysis of haadf-stem images," *Journal of Structural Biology*, vol. 166, no. 1, pp. 22 – 31, 2009.

11. J. S. Rohrer, Q. T. Islam, G. D. Watt, D. E. Sayers, and E. C. Theil, "Iron environment in ferritin with large amounts of phosphate, from *Azotobacter vinelandii* and horse spleen, analyzed using extended x-ray absorption fine structure (exafs)," *Biochemistry*, vol. 29, no. 1, pp. 259–264, 1990.

12. P. Mackle, C. D. Garner, R. J. Ward, and T. J. Peters, "Iron K-edge absorption spectroscopic investigations of the cores of ferritin and haemosiderins," *Biochim. Biophys. Acta*, vol. 1115, pp. 145–150, 1991.

13. S. L. Heath, J. M. Charnock, C. D. Garner, and A. K. Powell, "Extended X-ray Absorption Fine Structure (EXAFS) Studies of Hydroxo(oxo)iron Aggregates and Minerals, and a

Critique of their Use as Models for Ferritin," *Chem. - A Eur. J.*, vol. 2, no. 6, pp. 634–639, 1996.

14. G. S. Waldo, E. Wright, Z. H. Whang, J. F. Briat, E. C. Theil, and D. E. Sayers, "Formation of the ferritin iron mineral occurs in plastids.," *Plant Physiol.*, vol. 109, pp. 797–802, Nov. 1995.

15. M. Whitnall, Y. S. Rahmanto, M. L.-H. Huang, F. Saletta, H. C. Lok, L. Gutierrez, F. J. Lazaro, A. J. Fleming, T. G. S. Pierre, M. R. Mikhael, P. Ponka, and D. R. Richardson, "Identification of nonferritin mitochondrial iron deposits in a mouse model of friedreich ataxia," *Proceedings of the National Academy of Sciences*, vol. 109, pp. 20590–20595, Dec 2012.

16. L. A. Cohen, L. Gutierrez, A. Weiss, Y. Leichtmann-Bardoogo, D.-L. Zhang, D. R. Crooks, R. Sougrat, A. Morgenstern, B. Galy, M. W. Hentze, F. J. Lazaro, T. A. Rouault, and E. G. Meyron-Holtz, "Serum ferritin is derived primarily from macrophages through a nonclassical secretory pathway," *Blood*, vol. 116, pp. 1574–1584, Sep 2010.

17. F. Missirlis, S. Holmberg, T. Georgieva, B. C. Dunkov, T. A. Rouault, and J. H. Law, "Characterization of mitochondrial ferritin in drosophila," *Proceedings of the National Academy of Sciences*, vol. 103, no. 15, pp. 5893–5898, 2006.

18. N. Gálvez, B. Fernández, P. Sánchez, R. Cuesta, M. Ceolín, M. Clemente-León, S. Trasobares, M. López-Haro, J. J. Calvino, O. Stéphan, and J. M. Domínguez-Vera, "Comparative structural and chemical studies of ferritin cores with gradual removal of their iron contents," *J. Am. Chem. Soc.*, vol. 130, no. 25, pp. 8062–8, 2008.

19. T. S. Pierre, P. Chan, K. Bauchspiess, J. Webb, S. Betteridge, S. Walton, and D. Dickson, "Synthesis, structure and magnetic properties of ferritin cores with varying composition

and degrees of structural order: models for iron oxide deposits in iron-overload diseases," *Coord. Chem. Rev.*, vol. 151, no. 0, pp. 125 – 143, 1996.

20. F. M. Michel, H.-A. Hosein, D. B. Hausner, S. Debnath, J. B. Parise, and D. R. Strongin, "Reactivity of ferritin and the structure of ferritin-derived ferrihydrite," *Biochim. Biophys. Acta*, vol. 1800, no. 8, pp. 871–885, 2010.

21. A. Navrotsky, L. Mazeina, and J. Majzlan, "Size-driven structural and thermodynamic complexity in iron oxides," *Science*, vol. 319, no. 5870, pp. 1635–1638, 2008.

22. M. F. Hochella, S. K. Lower, P. A. Maurice, R. L. Penn, N. Sahai, D. L. Sparks, and B. S. Twining, "Nanominerals, mineral nanoparticles, and earth systems," *Science*, vol. 319, no. 5870, pp. 1631–1635, 2008.

23. V. A. Drits, B. A. Sakharov, A. L. Salyn, and A. Manceau, "Structural model for ferrihydrite," *Clay Miner.*, vol. 28, pp. 185–207, 1993.

24. F. M. Michel, L. Ehm, S. M. Antao, P. L. Lee, P. J. Chupas, G. Liu, D. R. Strongin, M. A. A. Schoonen, B. L. Phillips, and J. B. Parise, "The structure of ferrihydrite, a nanocrystalline material," *Science*, vol. 316, no. 5832, pp. 1726–1729, 2007.

25. F. M. Michel, V. Barron, J. Torrent, M. P. Morales, C. J. Serna, J.-F. Boily, Q. Liu, A. Ambrosini, A. C. Cismasu, and G. E. Brown, "Ordered ferrimagnetic form of ferrihydrite reveals links among structure, composition, and magnetism," *Proc. Natl. Acad. Sci.*, vol. 107, no. 7, pp. 2787–2792, 2010.

26. S. A. Makhlouf, F. T. Parker, and A. E. Berkowitz, "Magnetic hysteresis anomalies in ferritin," *Phys. Rev. B*, vol. 55, no. 22, pp. R14717–R14720, 1997.

27. J. R. Friedman, U. Voskoboynik, and M. P. Sarachik, "Anomalous magnetic relaxation in ferritin," *Phys. Rev. B*, vol. 56, p. 1079615, 1997.

28. J. G. E. Harris, J. E. Grimaldi, D. D. Awschalom, A. Chiolero, and D. Loss, "Excess spin and the dynamics of antiferromagnetic ferritin," *Phys. Rev. B*, vol. 60, p. 3453, 1999.

29. P. Doig, J. W. Austin, and T. J. Trust, "The *Helicobacter pylori* 19.6-Kilodalton Protein Is an Iron- Containing Protein Resembling Ferritin," *J. Bacterology*, vol. 175, no. 2, pp. 557–560, 1993.

30. H. Aitken-Rogers, C. Singleton, A. Lewin, A. Taylor-Gee, G. R. Moore, and N. Le Brun, "Effect of phosphate on bacterioferritin-catalysed iron(ii) oxidation," *J. Biol. Inorg. Chem.*, vol. 9, no. 2, pp. 161–170, 2004.

31. A. Kauko, A. T. Pulliainen, S. Haataja, W. Meyer-Klaucke, J. Finne, and A. C. Papageorgiou, "Iron incorporation in *Streptococcus suis* Dps-like peroxide resistance protein Dpr requires mobility in the ferroxidase center and leads to the formation of a ferrihydrite-like core.," *J. Mol. Biol.*, vol. 364, no. 1, pp. 97–109, 2006.

32. P. D. Griffiths, B. R. Dobson, G. R. Jones, and D. T. Clarke, "Iron in the basal ganglia in parkinson's disease. an in vitro study using extended x-ray absorption fine structure and cryo-electron microscopy," *Brain*, vol. 122, pp. 667–73, 1999.

33. L. Zecca, M. Youdim, P. Riederer, J. Connor, and R. Crichton, "Iron, brain ageing and neurodegenerative disorders," *Nat. Rev. Neurosci.*, vol. 5, no. 11, pp. 863–873, 2004.

34. T. Rouault, "The role of iron regulatory proteins in mammalian iron homeostasis and disease," *Nat. Chem. Biol.*, vol. 2, no. 8, pp. 406–414, 2006.

35. C. Quintana and L. Gutiérrez, "Could a dysfunction of ferritin be a determinant factor in the aetiology of some neurodegenerative diseases?," *Biochim. Biophys. Acta*, vol. 1800, no. 8, pp. 770–782, 2010.

36. A. Martelli and H. Puccio, "Dysregulation of cellular iron metabolism in friedreich ataxia: from primary iron-sulfur cluster deficit to mitochondrial iron accumulation," *Frontiers in Pharmacology*, vol. 5, no. 130, 2014.

37. S. Gider, D. Awschalom, T. Douglas, S. Mann, and M. Chaparala, "Classical and quantum magnetic phenomena in natural and artificial ferritin proteins," *Science*, vol. 268, no. 5207, pp. 77–80, 1995.

38. K.-I. Sano, A. Miura, S. Yoshii, M. Okuda, M. Fukuta, Y. Uraoka, T. Fuyuki, I. Yamashita, and K. Shiba, "Nonvolatile flash memory based on biologically integrated hierarchical nanostructures," *Langmuir*, vol. 29, no. 40, pp. 12483–12489, 2013.

39. M. Okuda, J.-C. Eloi, S. E. W. Jones, A. Sarua, R. M. Richardson, and W. Schwarzacher, "Fe3o4 nanoparticles: protein-mediated crystalline magnetic superstructures," *Nanotechnology*, vol. 23, p. 5601, 2012.

40. M. A. Kostiainen, P. Ceci, M. Fornara, P. Hiekkataipale, O. Kasyutich, R. J. M. Nolte, J. J. L. M. Cornelissen, R. D. Desautels, and J. van Lierop, "Hierarchical self-assembly and optical disassembly for controlled switching of magnetoferritin nanoparticle magnetism," *ACS Nano*, vol. 5, no. 8, pp. 6394–6402, 2011.

41. M. Suzuki, M. Abe, T. Ueno, S. Abe, T. Goto, Y. Toda, T. Akita, Y. Yamada, and Y. Watanabe, "Preparation and catalytic reaction of au/pd bimetallic nanoparticles in apo-ferritin," *Chem. Commun.*, pp. 4871 – 4873, 2009.

42. E. Fantechi, C. Innocenti, M. Zanardelli, M. Fittipaldi, E. Falvo, M. Carbo, V. Shullani, L. D. C. Mannelli, C. Ghelardini, and A. Ferretti, "A smart platform for hyperthermia application in cancer treatment: Cobalt-doped ferrite nanoparticles mineralized in human ferritin cages," *ACS Nano*, vol. 8, no. 5, pp. 4705–4719, 2014.

43. B. Bhushan, S. U. Kumar, I. Matai, A. Sachdev, P. Dubey, and P. Gopinath, "Ferritin nanocages: A novel platform for biomedical applications," *J. Biomed. Nanotechnol.*, vol. 10, no. 10, pp. 2950–2976, 2014.

44. M. Izuhara, K. Takamune, and R. Takata, "Cloning and sequencing of an *Escherichia coli* K12 gene which encodes a polypeptide having similarity to the human ferritin H subunit," *Molecular and General Genetics MGG*, vol. 225, no. 3, pp. 510–513, 1991.

45. S. C. Andrews, P. M. Harrison, and J. R. Guest, "Cloning, sequencing, and mapping of the bacterioferritin gene (bfr) of *Escherichia coli* K-12," *J Bacteriol*, vol. 171, no. 7, pp. 3940–7, 1989.

46. O. Kasyutich, A. Ilari, A. Fiorillo, D. Tatchev, A. Hoell, and P. Ceci, "Silver ion incorporation and nanoparticle formation inside the cavity of *Pyrococcus furiosus* ferritin: structural and size-distribution analyses," *J. Am. Chem. Soc.*, vol. 132, no. 10, pp. 3621–7, 2010.

47. R. M. Cornell and U. Schwertmann in *The iron oxides: Structure, Properties, Reactions, Ocurences and Uses*, Wiley-VCH Verlag GmbH and Co., Weinheim.

48. F. Brem, G. Stamm, and A. M. Hirt, "Modeling the magnetic behavior of horse spleen ferritin with a two-phase core structure," *J. Appl. Phys.*, vol. 99, no. 12, p. 123906, 2006.

49. R. J. Pollard, "Characterization of feooh polymorphs and ferrihydrite using low-temperature, applied-field, mossbauer spectroscopy," *Clay Minerals*, vol. 27, pp. 57–71, 1992.

50. M. Wilke, F. Farges, P. Petit, G. Brown, and F. Martin, "Oxidation state and coordination of Fe in minerals : An Fe K-XANES spectroscopic study," *Am. Mineral.*, vol. 86, pp. 714–730, 2001.

51. A. Voegelin, R. Kaegi, J. Frommer, D. Vantelon, and S. J. Hug, "Effect of phosphate, silicate, and Ca on Fe(III)-precipitates formed in aerated Fe(II)- and As(III)-containing water studied by X-ray absorption spectroscopy," *Geochim. Cosmochim. Acta*, vol. 74, no. 1, pp. 164–186, 2010.

52. J. Baumgartner, G. Morin, N. Menguy, T. Perez Gonzalez, M. Widdrat, J. Cosmidis, and D. Faivre, "Magnetotactic bacteria form magnetite from a phosphate-rich ferric hydroxide via nanometric ferric (oxyhydr)oxide intermediates.," *Proc. Natl. Acad. Sci. U. S. A.*, vol. 1, no. 20, pp. 1–6, 2013.

53. D. Koningsberger and R. Prins, *X-Ray Absorption: Principles, Applications, Techniques of EXAFS, SEXAFS and XANES*. New York: Wiley-Interscience, 1988.

54. C. M. van Genuchten, J. Peña, S. E. Amrose, and A. J. Gadgil, "Structure of Fe(III) precipitates generated by the electrolytic dissolution of Fe(0) in the presence of groundwater ions," *Geochim. Cosmochim. Acta*, vol. 127, pp. 285–304, 2014.

55. G. A. Waychunas, C. C. Fuller, and J. A. Davis, "Surface complexation and precipitate geometry for aqueous Zn (II) sorption on ferrihydrite I : X-ray absorption extended fine structure spectroscopy analysis," *Geochim. Cosmochim. Acta*, vol. 66, no. 7, pp. 1119–1137, 2002.

56. C. Mikutta, "X-ray absorption spectroscopy study on the effect of hydroxybenzoic acids on the formation and structure of ferrihydrite," *Geochim. Cosmochim. Acta*, vol. 75, no. 18, pp. 5122–5139, 2011.

57. A. I. Frenkel, A. Yevick, C. Cooper, and R. Vasic, "Modeling the structure and composition of nanoparticles by extended x-ray absorption fine-structure spectroscopy," *Annual Review of Analytical Chemistry*, vol. 4, no. 1, pp. 23–39, 2011.

58. N. Rinaldi-Montes, D. Martínez-Blanco, A. B. Fuertes, L. F. Barquín, J. R. Fernández, I. de Pedro, M. L. Fdez-Gubieda, J. Alonso, L. Olivi, G. Aquilantie, and J. A. Blanco, "Interplay between microstructure and magnetism in nio nanoparticles: breakdown of the antiferromagnetic order," *Nanoscale*, vol. 6, p. 457, 2014.

59. F. Maillot, G. Morin, Y. Wang, D. Bonnin, P. Ildefonse, C. Chaneac, and G. Calas, "New insight into the structure of nanocrystalline ferrihydrite: Exafs evidence for tetrahedrally coordinated iron(iii)," *Geochim. Cosmichim. Ac.*, vol. 75, no. 10, pp. 2708 – 2720, 2011.

60. M. L. Fdez-Gubieda, A. Muela, J. Alonso, A. García-Prieto, L. Olivi, R. Fernández-Pacheco, and J. M. Barandiarán, "Magnetite biomineralization in *Magnetospirillum gryphiswaldense*: Time-resolved magnetic and structural studies," *ACS Nano*, vol. 7, no. 4, pp. 3297–305, 2013.

61. T. S. Pierre, J.Webb, and S. Mann, "Ferritin and Hemosiderin: structural and magnetic studies of the iron core," in *Biomineralization: Chemical and Biochemical perspectives* (R. W. S. Mann, J. Webb, ed.), pp. 295–344, Verlagsgesellschaft, Weinheim, 1989.

Supplementary Information
On the mineral core of ferritin-like proteins: from archaea to mammals

A. García-Prieto[1,2], J. Alonso[2,3], D. Muñoz[4,5],
L. Marcano[5], A. Abad Díaz de Cerio[4,5], R. Fernández de Luis[2],
I. Orue[6], O. Mathon[7], A. Muela[2,4], M.L. Fdez-Gubieda[2,5]

[1] Dpto. de Física Aplicada I, Universidad del País Vasco - UPV/EHU, 48013 Bilbao, Spain
[2] BCMaterials, Parque tecnológico de Zamudio, 48160 Derio, Spain
[3] Department of Physics, University of South Florida, Tampa, FL 33647, USA
[4] Dpto. de Inmunología, Microbiología y Parasitología,
Universidad del País Vasco - UPV/EHU, 48940 Leioa, Spain
[5] Dpto. de Electricidad y Electrónica, Universidad del País Vasco - UPV/EHU, 48940 Leioa, Spain
[6] SGIker, Universidad del País Vasco UPV/EHU, 48940 Leioa, Spain
[7] European Synchrotron Radiation Facility, 38000 Grenoble, France

October 9, 2015

1 EXAFS analysis

We have measured the XANES spectrum of the FeIII-citrate. As it can be observed in figure 1, the XANES is completely different to that measured in prokaryotic samples.

We have also measured the XAFS spectra of the wild-type *E. coli* (control) grown in non-supplemented and iron supplemented media. Even though the repletion in both cases could be different, the XANES and EXAFS spectra are similar, see figure 2. As expected, we do not detect any change on the structure.

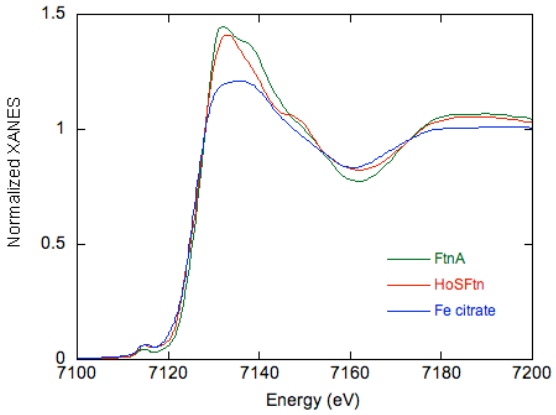

Figure 1: XANES spectra of Fe citrate compare with

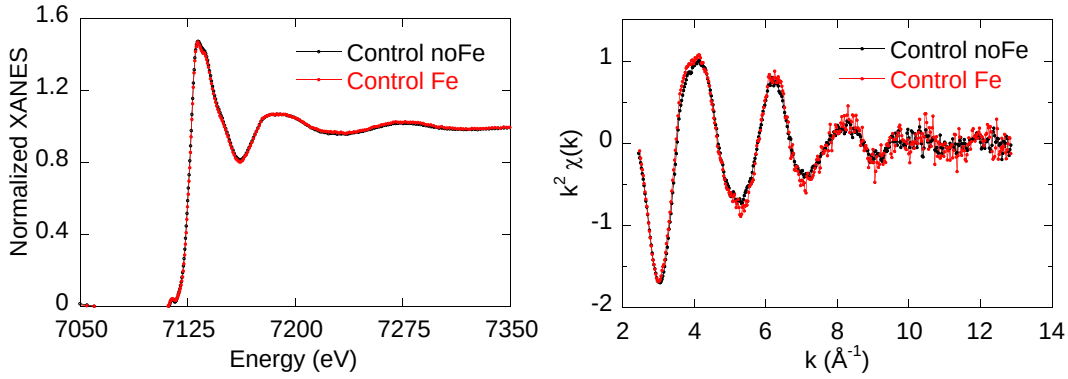

Figure 2: XANES spectra (left) and EXAFS spectra (right) of non-overexpressing *E. coli* DH5α (control) grown in non-supplemented and iron supplemented media

EXAFS spectra of the studied samples have been fitted to the expression: (*1*)

$$k\chi(k) = \sum_j S_0^2 N_j f_j(k,\pi) \frac{e^{-2\sigma_j^2 k^2} e^{-2\Gamma_j/k}}{R_j^2} \sin[2kR_j + \phi_j(k,\pi)]. \quad (1)$$

The sum expands over all the species of backscattering atoms at the same distance R_j of the central atom with variance σ_j^2 (Debye-Waller factor) around the absorber, and N_j is the number of such atoms. The scale factor S_0^2 is related to the many body effects and $e^{-2\Gamma_j/k}$ is a mean free path term that takes into account the inelastic losses of the photoelectron. $f_j(k,\pi)$ is the magnitude of the effective curved-wave backscattering amplitude for the jth type of atoms and $\phi_j(k,\pi) = (2\delta(k) - \pi) + \Phi_j(k)$, where the first and second terms represent the modification in the phase shift of the ejected photoelectron wave function by the potential of the central absorbing and backscattering atoms, respectively. In our case, the central atom is Fe and two types of scattering atoms have been taken into account: O and Fe and additionally P for the prokaryotic ferritins. The corresponding backscattering parameters $f(k,\pi)$, and $\phi(k,\pi)$ have been theoretically generated with the FEFF6.0 codes. (*2*) The fitting has been performed on the R space in 0 Å$\leq R \leq$ 3.5 Å. The fitting procedure consists on the minimization of the difference between the Fourier filtered experimental data $\chi_{exp}^F(k)$ and the model function $\chi_{th}(k)$. The function to minimize is defined as

$$S^2 = \frac{\sum_{i=1}^N [k_i^2 \chi_{exp}^F(k_i) - k_i^2 \chi_{th}(k_i)]^2}{\sum_{i=1}^N [k_i^2 \chi_{exp}^F(k_i)]^2} \quad (2)$$

In order to improve the reliability of the fits, the four samples have been fitted simultaneously as implemented in the IFeffit and Artemis softwares (*3,4*). The parameters S_0^2 and ΔE for each path were left free in the fitting procedure but were common for all the samples, resulting in a value of $S_0^2 = 0.8$. Results have been checked with the additional XAFS software Viper (*5*).

An attempt of fitting the EXAFS data to an amorphous function was made. In this case, the corresponding fitting expression in the framework of a the dense random packing model of hard spheres (*6*) is:

$$k\chi(k) = \sum_j S_0^2 N_j f_j(k) \frac{e^{-2\sigma_j^2 k^2} e^{-2\Gamma_j/k}}{R_j^2} \frac{1}{\sqrt{1+4k^2\sigma_{Dj}^2}} \sin\left[2kR_j + \arctan\left(2k\sigma_{DJ}\right) + \varphi_j(k)\right] \tag{3}$$

In this model, R_j is the distance between the centers of two touching spheres, and σ_{Dj} is the root mean square deviation of the distance between the absorbing atom and the neighbour j. This expression has proved to be very useful in the analysis of amorphous alloys, such as $(Fe_{0.2}Co_{0.8})_{75}Si_xB_{25-x}$, Co-P or Fe-B (*7–10*).

2 Transmission Electron Microscopy (TEM)

In figure**??** we show the TEM images taken at a PHILIPS CM120 microscope at the University of Basque Country, working at 120 kV for the wild-type *E.coli* (control), overexpressing bacterial ferritin (FTnA) and bacterioferritin (Bfr) grown in iron supplemented media. TEM analysis show isolated dense spots all over the cytoplasm in FtnA overexpressing cells and dense aggregates closed to the cytoplasmic membrane in Bfr overexpressing cells. However, this kind of dense spots and aggregates are not seen in the non-overexpressing E. coli DH5α. For HRTEM analysis we have focused on this particular events.

The lattice spacings and angular relationships obtained by the Fourier transform of HRTEM images of the HoSF have been compared with the theoretically generated patterns obtained from the defective free ferrihydrite model proposed by V.A. Drits and co-workers (*11*), Figure 4. Two possible zone axis, [1,1,1] and [0,1,1] have been correlated with the experimental data. Both of them possess four reflections with lattice spacing (2.43 Å, 2.39 Å) near the calculated value (2.47 Å), and two more with higher lattice spacing (2.50 Å) near the 2.56 Åvalue. The experimental angles (62° and 60°) also match with the theoretical ones (61.16° and 57.88°). The deviations between the experimental and theoretical data could be explained taking into

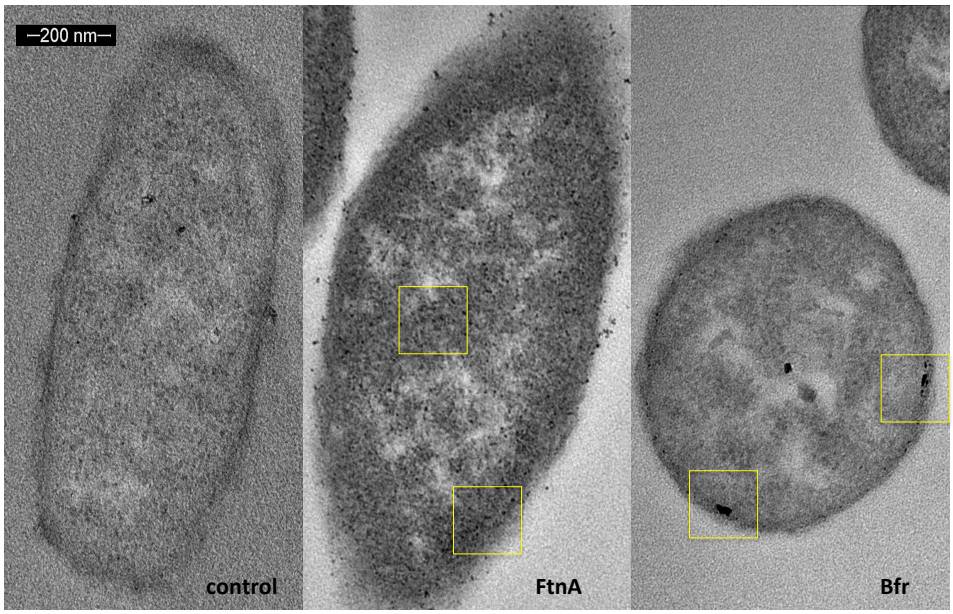

Figure 3: TEM images of the non-overexpressing *E.coli* (control), overexpressing bacterial ferritin (FTnA) and bacterioferritin (Bfr). The cells were grown in iron supplemented medium.

account that the ferritin cores are not exactly oriented in a zone axis. There is no possibility to identify exactly the zone axis in which the cores of the HoSF are oriented. Two HRTEM images in different zone axis, taken in the same HoSF core, are needed for this purpose. Nevertheless, the experimental and simulated patterns indicate that the nature of HoSF cores in related to the ferrihydrite.

The Figure 5a shows the Fourier transform of the bacterial ferritin core. The lattice spacings and angles between them are clearly different from those obtained for the HoSF. The Figure 5b indicates the mean spacing values and angle relationships between the spots observed in the Fourier transform image for the bacterial ferritin core.

3 Magnetic characterization

In a case of a paramagnet compound, Fe^{3+} should contribute with 5 μ_B which corresponds to a magnetic moment given by $J = 5/2$ and $g = 2$ (μ= gJ μ_B) In fact, this point has been confirmed by the fact that the magnetic data, M(H) and M(T), follow nicely a Brillouin function given by:

$$M = M_0 \frac{2J+1}{2J} \coth\left(\frac{2J+1}{2J}\frac{gJ\mu_B H}{k_B T}\right) - \frac{1}{2J}\coth\left(\frac{1}{2J}\frac{gJ\mu_B H}{k_B T}\right) + \chi H \qquad (4)$$

References

1. E. A. Stern *Contemp. Phys.*, vol. 19, no. 4, pp. 289–310, 1978.

2. S. I. Zabinsky, J. J. Rehr, A. Ankudinov, R. C. Albers, and M. J. Eller, "Multiple-scattering calculations of x-ray-absorption spectra," *Phys. Rev. B*, vol. 52, pp. 2995–3009, Jul 1995.

3. M. Newville, "*IFEFFIT*: interactive XAFS analysis and *FEFF* fitting," *J. Synchrotron Rad.*, vol. 8, pp. 322–324, Mar 2001.

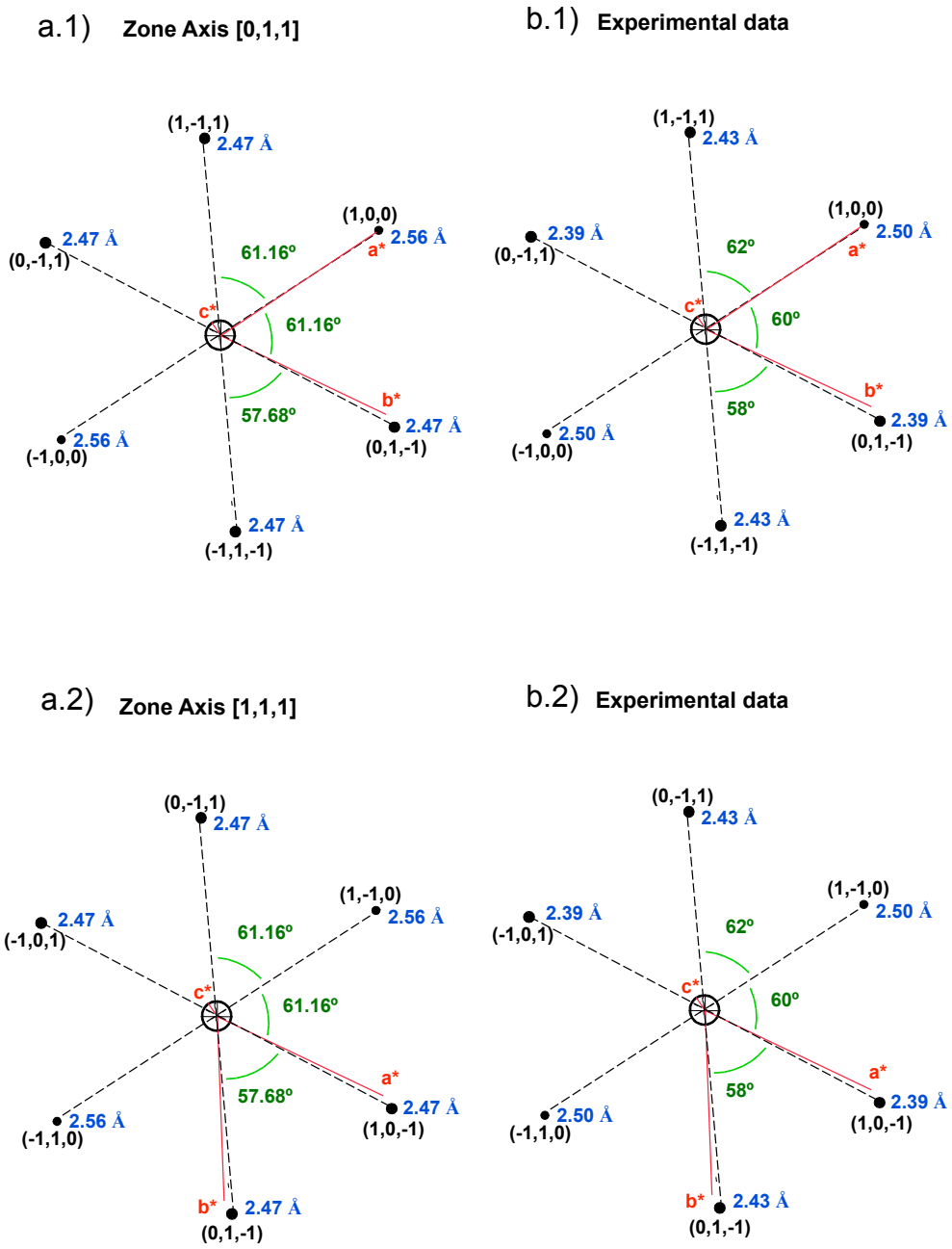

Figure 4: (a.1)-(a.2) Theoretical diffraction patterns for the defective free ferrihydrite, zone axis $[1,1,1]$ (a.1) and $[0,1,1]$ (a.2). (b.1)-(b.2) Spots of the Fourier transform of the HoSF indexed for a defective free ferrihydrite model in the $[1,1,1]$ (b.1) and $[0,1,1]$ zone axis.

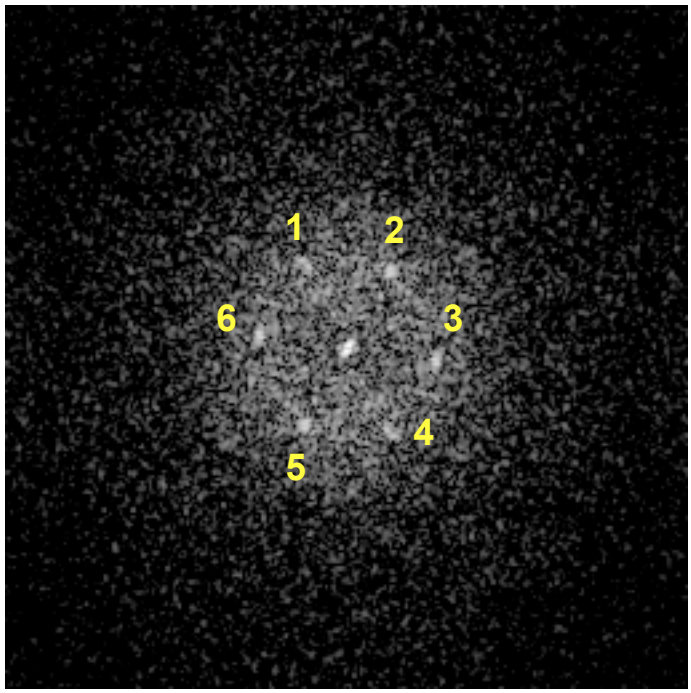

d_1(Å)	d_2 (Å)	angle°
2.88	2.87	68.0
d_2 (Å)	d_3(Å)	
2.87	2.57	55.8
d_3(Å)	d_4(Å)	
2.57	2.88	56.1
d_4(Å)	d_5 (Å)	
2.88	2.87	68.2
d_5(Å)	d_6(Å)	
2.88	2.57	55.8
d_6(Å)	d_1(Å)	
2.57	2.88	56.1

Figure 5: a) Fourier transform of the bacterial ferritin core. b) d spacing and angles for the observed spots.

4. B. Ravel and M. Newville, "*ATHENA*, *ARTEMIS*, *HEPHAESTUS*: data analysis for X-ray absorption spectroscopy using *IFEFFIT*," *J. Synchrotron Rad.*, vol. 12, pp. 537–541, Jul 2005.

5. K. V. Klementev, "Extraction of the fine structure from x-ray absorption spectra," *J. Phys. D Appl. Phys.*, vol. 34, no. 2, p. 209, 2001.

6. M. D. Crescenzi, A. Balzarotti, F. Comin, L. Incoccia, S. Mobilio, and N. Motta, "Exafs measurements on feb metallic glasses: Asymmetry of the radial distribution function," *Solid State Commun.*, vol. 37, no. 12, pp. 921 – 923, 1981.

7. M. L. Fdez-Gubieda, I. Orúe, F. Plazaola, and J. M. Barandiarán, "Evidence of strong short-range order in (fe0.2co0.8)75sixb25-x amorphous alloys from exafs spectroscopy," *Phys. Rev. B*, vol. 53, pp. 620–628, Jan 1996.

8. M. Fdez-Gubieda, A. García-Arribas, J. Barandiarán, R. López Antón, I. Orue, P. Gorria, S. Pizzini, and A. Fontaine, "Local structure and ferromagnetic character of fe-b and fe-p amorphous alloys," *Phys. Rev. B*, vol. 62, pp. 5746–5750, Sep 2000.

9. M. L. Fdez-Gubieda, A. García-Arribas, I. Orue, F. Plazaola, and J. M. Barandiarán, "Medium-range order as an intrinsic property of co-rich amorphous alloys," *Europhys. Lett.*, vol. 40, no. 1, p. 43, 1997.

10. A. García-Arribas, M. Fdez-Gubieda, and J. Barandiarán, "Comparative study of the structure and magnetic properties of co-p and fe-p amorphous alloys," *Phys. Rev. B*, vol. 61, pp. 6238–6245, Mar 2000.

11. V. A. Drits, B. A. Sakharov, A. L. Salyn, and A. Manceau, "Structural model for ferrihydrite," *Clay Miner.*, vol. 28, pp. 185–207, 1993.